Beamforming with Infineon BGT60TR13C

Sultanus Salehin

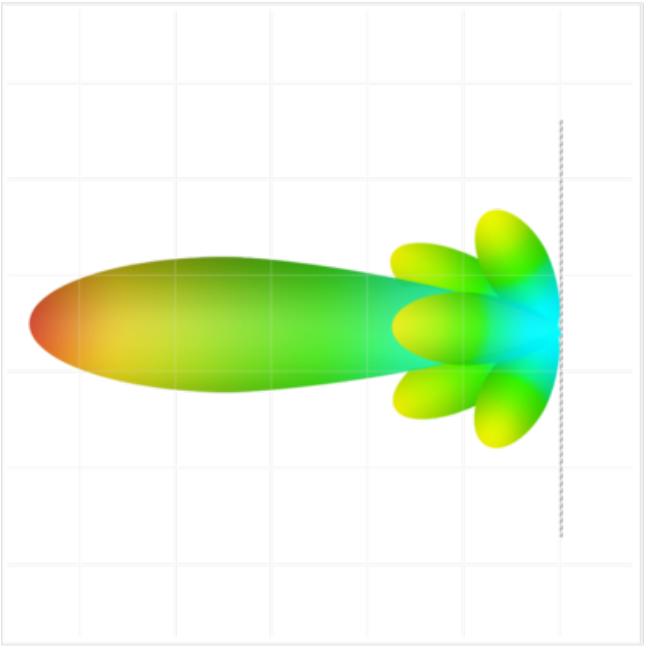

Contents

1 Radar Signal Model

The Infineon BGT60TR13C is a compact **single-transmit (TX), three-receive (RX)** mmWave FMCW radar. Beamforming and DOA estimation on this platform rely entirely on the **relative phase differences** observed across the three RX channels at a given range bin. This section derives the FMCW baseband model used in the code and explains how the sampled data becomes the spatial snapshots that feed covariance estimation and beamforming.

1.1 Transmit FMCW Chirp and Dechirped Beat Signal

An FMCW radar transmits a linear frequency-modulated chirp. A common complex baseband representation for the transmitted waveform is

$$s_{\text{tx}}(t) = \exp\left(j2\pi\left(f_0 t + \frac{S}{2}t^2\right)\right), \quad 0 \le t \le T_c, \tag{1}$$

where f_0 is the start (carrier) frequency, S is the chirp slope (Hz/s), and T_c is the chirp duration.

Consider a single point target at range R (round-trip delay $\tau = \frac{2R}{c}$). Neglecting Doppler for the moment, the received signal at RX element m can be modeled as a delayed and scaled copy:

$$s_{\text{rx},m}(t) \approx \alpha_m \, s_{\text{tx}}(t - \tau), \tag{2}$$

where α_m is a complex gain that includes propagation loss, target reflectivity, and any per-channel phase/amplitude imbalance.

FMCW radars typically form the **dechirped** (or "beat") signal by mixing the received signal with a conjugated copy of the transmitted chirp:

$$x_m(t) = s_{\text{rx},m}(t) \, s^*_{\text{tx}}(t). \tag{3}$$

Substituting (1) and simplifying yields (up to a constant phase term) a complex sinusoid at the **beat frequency**:

$$x_m(t) \approx \alpha_m \exp(j2\pi f_b t), \quad f_b = S\tau = \frac{2SR}{c}. \tag{4}$$

Key point: range is encoded as frequency in the dechirped signal. A target at a larger R produces a larger f_b.

1.2 Array Geometry and Angle-Dependent Phase

The BGT60TR13C has three RX antennas arranged approximately as a **uniform linear array (ULA)** with inter-element spacing d. Assuming far-field propagation, a plane wave arriving from azimuth angle θ produces a **deterministic phase progression** across the array.

Let the RX elements be indexed by $m \in \{0, 1, \ldots, M-1\}$ with $M = 3$. For a ULA, the additional path length from element m relative to element 0 is approximately

$$\Delta\ell_m(\theta) \approx md\sin(\theta), \tag{5}$$

which corresponds to a phase shift

$$\phi_m(\theta) = \frac{2\pi}{\lambda}\Delta\ell_m(\theta) = 2\pi\frac{md}{\lambda}\sin(\theta). \tag{6}$$

Incorporating this spatial phase into the dechirped beat model (4) gives the continuous-time signal model used for beamforming:

$$x_m(t) = \alpha\, e^{j2\pi f_b t}\, e^{j2\pi\frac{md}{\lambda}\sin(\theta)}. \tag{7}$$

Interpretation:

- $e^{j2\pi f_b t}$ encodes **range** (via beat frequency).
- $e^{j2\pi\frac{md}{\lambda}\sin(\theta)}$ encodes **angle** (via relative phase across RX channels).
- Beamforming/DOA methods work by comparing observed phase relationships across the RX channels to those predicted by (6).

1.3 Discrete-Time Sampling: From ADC to Range Bins

Each chirp is sampled by the ADC at rate f_s producing N_s complex samples per chirp. Let $n \in \{0, 1, \ldots, N_s - 1\}$ index fast-time samples within a chirp:

$$x_m[n] = x_m(t)\big|_{t=n/f_s}. \tag{8}$$

For a single chirp, the standard range processing step is the **fast-time FFT**:

$$X_m[k] = \sum_{n=0}^{N_s-1} x_m[n]\; w[n]\; e^{-j2\pi kn/N_s}, \quad k = 0, \ldots, N_s - 1, \tag{9}$$

where $w[n]$ is a window function (e.g., Hann) to reduce sidelobes.

Each FFT bin k corresponds to a beat frequency $f_k = \frac{kf_s}{N_s}$, and thus to a range

$$R_k \approx \frac{c}{2S}f_k = \frac{c}{2S}\frac{kf_s}{N_s}. \tag{10}$$

In practice, the code uses a precomputed range resolution (from radar parameters), so the range axis is treated as

$$R_k \approx k\,\Delta R, \tag{11}$$

with ΔR determined by bandwidth and signal processing configuration.

1.4 Spatial Snapshot at a Range Bin (What Beamforming Uses)

After performing the range FFT, for a fixed range bin r (FFT index $k = r$), we can form the **spatial snapshot vector** by stacking the RX FFT outputs:

$$x[r] = \begin{bmatrix} X_0[r] \\ X_1[r] \\ \vdots \\ X_{M-1}[r] \end{bmatrix} \in \mathbb{C}^{M\times 1}. \tag{12}$$

This snapshot is computed repeatedly across slow-time (chirps) and/or across CPIs, which provides multiple realizations

$$x_1[r], x_2[r], \ldots, x_N[r],$$

used to estimate the covariance matrix in the next stage of the pipeline.

Pipeline linkage to the code:

- `preprocess_frame()` performs DC removal, windowing, and the FFT (9).
- It outputs a data cube indexed as `cube[range, chirp, rx]`.
- For a fixed range bin r, the slow-time snapshots correspond to `cube[r, :, :]` which is an $N_{\text{chirps}} \times M$ matrix.
- The covariance estimation stage treats each chirp (or CPI-averaged chirps) as a sample $x_n[r]$ and builds $R(r)$.

1.5 Multi-Target Extension (Why Multiple Peaks Appear)

For K targets located at ranges R_k and angles θ_k, the received snapshot at a fixed range bin (ideally aligned to one target) can be modeled as a superposition:

$$x[r] \approx \sum_{k=1}^{K} \alpha_k(r)\, a(\theta_k) + n[r], \tag{13}$$

where $n[r]$ is noise and $a(\theta)$ is the steering vector (defined in a later section).

In real indoor measurements, **multipath** and **range sidelobes** cause energy from a single physical reflector to leak into neighboring range bins and appear as additional components in (13). This effect is a major reason why MUSIC can show multiple blobs/peaks even when the number of true reflectors is small.

1.6 Modeling Assumptions and Practical Violations

The model in (7) relies on the following assumptions:

- **Far-field (plane-wave) assumption:** the wavefront is planar across the array aperture.
- **Narrowband assumption at each range bin:** within one bin, the steering vector is well-defined and frequency-independent.
- **Perfect calibration:** RX channels have matched phase and gain.
- **Negligible mutual coupling:** antennas do not distort each other's responses.

For compact radars like the BGT60TR13C, several of these assumptions are often violated:

- The target may be **near-field** at short ranges, making the plane-wave model inaccurate.
- RX gain/phase mismatches and mutual coupling distort the effective array manifold.
- Multipath in indoor environments introduces coherent arrivals, which breaks ideal subspace separation.

These violations do not prevent beamforming, but they significantly reduce the reliability and interpretability of high-resolution methods such as MUSIC, especially with only $M = 3$ RX channels.

2 Spatial Covariance Estimation

All beamforming and DOA estimation methods implemented in this work rely on an estimate of the **spatial covariance matrix** at each range bin. This matrix captures the spatial correlation between the RX antenna elements and encodes all angular information available to the array.

2.1 Sample Covariance Matrix

For a fixed range bin r, let

$$x_n(r) \in \mathbb{C}^{M\times 1}, \quad n = 1, 2, \ldots, N,$$

denote the spatial snapshot vectors extracted across slow time (chirps) and possibly across multiple CPIs. The sample covariance matrix is estimated as

$$R(r) = \frac{1}{N} \sum_{n=1}^{N} x_n(r)\, x_n^H(r), \tag{14}$$

where

- M is the number of RX antennas (here $M = 3$),
- $N = N_{\text{chirps}} \times N_{\text{CPI}}$ is the total number of snapshots used,
- $(\cdot)^H$ denotes the Hermitian (conjugate transpose).

Each element of $R(r)$ has a clear interpretation:

$$[R(r)]_{i,j} = \mathbb{E}\{x_i(r)\, x_j^*(r)\}, \tag{15}$$

which measures the cross-correlation between RX channels i and j at range bin r.

Key insight: All angular information used by Bartlett, MVDR, and MUSIC is contained in the *off-diagonal phase relationships* of $R(r)$.

2.2 Connection to the Signal Model

Under the multi-target model introduced in Section 2,

$$x_n(r) \approx \sum_{k=1}^{K} \alpha_{k,n}(r)\, a(\theta_k) + n_n(r), \tag{16}$$

the covariance matrix can be written (approximately) as

$$R(r) \approx \sum_{k=1}^{K} \sigma_k^2(r)\, a(\theta_k) a^H(\theta_k) + \sigma_n^2 I, \tag{17}$$

where $a(\theta_k)$ is the array steering vector and $\sigma_k^2(r)$ represents signal power contributions.

This structure is what enables:

- Bartlett to measure directional power,
- MVDR to suppress interference,
- MUSIC to separate signal and noise subspaces.

2.3 Snapshot Formation in the Pipeline

In the implemented pipeline:

- Each chirp provides one spatial snapshot per range bin.
- Snapshots are extracted from the FFT cube as `cube[r, chirp, rx]`.
- If multiple CPIs are available, snapshots from different CPIs are concatenated or averaged.

This produces the snapshot set

$$\{x_1(r), x_2(r), \ldots, x_N(r)\},$$

which is used to compute $R(r)$ via (14).

Practical limitation: With only $M = 3$ RX channels, reliable covariance estimation requires a sufficiently large N. When N is small, $R(r)$ becomes noisy or ill-conditioned, directly degrading MVDR and MUSIC performance.

2.4 Slow-Time Mean Removal (Clutter Suppression)

Stationary reflectors (walls, furniture, static objects) produce strong, nearly constant returns across chirps. These contributions dominate the covariance matrix and obscure angular information.

To suppress such clutter, the slow-time mean is removed prior to covariance estimation:

$$\tilde{x}_n(r) = x_n(r) - \frac{1}{N}\sum_{k=1}^{N} x_k(r). \tag{18}$$

This operation acts as a **zero-Doppler high-pass filter** in slow time, analogous to classical MTI filtering.

Effect:

- Suppresses stationary clutter,
- Improves angular contrast for moving or isolated targets,
- Reduces rank inflation in the covariance matrix.

2.5 CPI Averaging (Snapshot Averaging)

When multiple CPIs are available, covariance matrices can be computed independently for each CPI and then averaged:

$$R_{\text{avg}}(r) = \frac{1}{N_{\text{CPI}}}\sum_{c=1}^{N_{\text{CPI}}} R^{(c)}(r). \tag{19}$$

This averaging:

- Increases the effective number of snapshots,
- Reduces variance in covariance estimates,
- Improves numerical stability for matrix inversion and eigendecomposition.

Trade-off: CPI averaging assumes scene stationarity across CPIs. Rapidly changing targets or motion between CPIs can violate this assumption.

2.6 Hermitian Enforcement

In theory, the covariance matrix $R(r)$ is Hermitian and positive semidefinite. In practice, finite precision arithmetic and limited snapshots introduce small asymmetries:

$$R(r) \neq R^H(r).$$

To ensure physically valid eigenstructure, explicit Hermitian enforcement is applied:

$$R(r) \leftarrow \frac{1}{2}\left(R(r) + R^H(r)\right). \tag{20}$$

This step:

- Guarantees real eigenvalues,
- Improves numerical robustness,
- Stabilizes MUSIC subspace separation and MVDR inversion.

2.7 Why Covariance Quality Matters (Critical Insight)

The accuracy of $R(r)$ directly determines beamforming performance:

- **Bartlett** is relatively insensitive to covariance errors.
- **MVDR** requires well-conditioned $R(r)$ for stable inversion.
- **MUSIC** is extremely sensitive to eigenvalue separation and rank estimation.

With only $M = 3$ RX elements on the BGT60TR13C, covariance estimation errors are a **primary limiting factor**, explaining:

- Spurious MUSIC peaks,
- Inconsistent MVDR sidelobe behavior,
- Strong dependence on snapshot count and clutter suppression.

3 Beamforming Methods

This section describes the three beamforming and DOA estimation techniques implemented in this work: Bartlett (conventional beamforming), MVDR (Capon beamforming), and MUSIC (subspace-based DOA estimation). All methods operate on the spatial covariance matrix $R(r)$ estimated at each range bin, as described in Section 3.

3.1 Bartlett (Conventional Beamforming)

The Bartlett beamformer, also known as *conventional* or *delay-and-sum* beamforming, computes the spatial power spectrum as

$$P_{\text{Bartlett}}(\theta) = a^H(\theta)\, R\, a(\theta), \tag{21}$$

where $a(\theta) \in \mathbb{C}^{M\times 1}$ is the array steering vector corresponding to look direction θ.

Interpretation

Equation (21) measures the output power obtained by steering the array toward angle θ and projecting the spatial covariance matrix onto that direction. Equivalently, Bartlett beamforming computes the correlation between the observed spatial field and a hypothesized plane wave arriving from angle θ.

From a geometric perspective:

- $a(\theta)$ defines a direction in the M-dimensional sensor space,
- $P_{\text{Bartlett}}(\theta)$ measures how much energy in R lies along that direction.

No attempt is made to suppress interference or noise arriving from other directions.

Properties

- **Non-adaptive:** weights do not depend on the interference environment.
- **Always stable:** no matrix inversion or eigenvalue decomposition is required.
- **Smooth response:** produces continuous and visually interpretable range–angle maps.
- **Resolution-limited:** angular resolution is constrained by the physical array aperture.

Behavior on the BGT60TR13C

With only $M = 3$ RX elements:

- The Bartlett mainlobe is inherently wide.
- Closely spaced targets cannot be resolved.
- Sidelobes are relatively high but stable.

For this radar, Bartlett beamforming serves primarily as a **baseline and sanity-check method** rather than a high-resolution DOA estimator.

3.2 MVDR / Capon Beamformer

The Minimum Variance Distortionless Response (MVDR), or Capon beamformer, designs spatial weights by solving the constrained optimization problem

$$\min_{w} \; w^H R w \quad \text{s.t.} \quad w^H a(\theta) = 1, \tag{22}$$

where w is the beamforming weight vector.

The constraint enforces unit gain in the desired look direction θ, while the objective minimizes output power due to noise and interference.

Closed-form solution

Solving (22) yields the MVDR spatial spectrum

$$P_{\text{MVDR}}(\theta) = \frac{1}{a^H(\theta)\, R^{-1}\, a(\theta)}. \tag{23}$$

Large values of $P_{\text{MVDR}}(\theta)$ indicate angles consistent with the observed covariance structure while suppressing energy from other directions.

Interpretation

MVDR is an **adaptive beamformer**:

- It shapes its spatial response based on R.
- Spatial nulls are placed in directions associated with strong interference or clutter.
- The beamwidth is narrower than Bartlett when covariance estimation is reliable.

Intuitively:

> Bartlett listens everywhere equally; MVDR listens carefully and suppresses what it does not need.

Practical considerations

Because R is estimated from finite data, it may be ill-conditioned or nearly singular. In practice, diagonal loading is applied before inversion:

$$R_{\text{loaded}} = R + \epsilon I, \tag{24}$$

where ϵ is chosen adaptively based on noise or SNR estimates.

Behavior on the BGT60TR13C

With $M = 3$ RX elements:

- MVDR provides modest resolution improvement over Bartlett.
- Performance is highly sensitive to snapshot count and clutter suppression.
- Poor covariance estimation leads to unstable sidelobes and distorted peaks.

Thus, MVDR offers **incremental improvement**, but remains fundamentally aperture-limited.

3.3 MUSIC (Subspace-Based DOA Estimation)

The MUltiple SIgnal Classification (MUSIC) algorithm is a subspace-based DOA estimation technique that exploits the eigenstructure of the spatial covariance matrix.

Subspace decomposition

Under the narrowband array model, the covariance matrix can be decomposed as

$$R = E_s \Lambda_s E_s^H + E_n \Lambda_n E_n^H, \tag{25}$$

where:

- E_s contains eigenvectors associated with the dominant (signal) eigenvalues,
- E_n contains eigenvectors associated with the smaller (noise) eigenvalues,
- E_s and E_n span orthogonal subspaces.

MUSIC pseudospectrum

The MUSIC pseudospectrum is defined as

$$P_{\text{MUSIC}}(\theta) = \frac{1}{\|E_n^H a(\theta)\|^2}. \tag{26}$$

At a true direction of arrival, the steering vector $a(\theta)$ lies in the signal subspace and is therefore orthogonal to the noise subspace, causing the denominator to approach zero and producing a sharp peak.

Key characteristics

- MUSIC does **not estimate power**; it estimates spatial consistency.
- Peak height is not proportional to target strength.
- Very narrow peaks ("super-resolution") are expected even for weak targets.

Critical limitations on the BGT60TR13C

For $M = 3$ RX elements:

- Maximum resolvable sources: $M - 1 = 2$.
- Any additional reflectors or multipath components violate the model.
- Near-field effects and calibration errors distort the signal subspace.

As a result, MUSIC often produces:

- Multiple sharp peaks per range bin,
- Spurious blobs in range–angle maps,

- High sensitivity to snapshot count and preprocessing.

These effects should not be interpreted as true targets, but rather as artifacts of applying a super-resolution algorithm to a severely aperture-limited array.

4 Angle Convention and Steering Vector Definition

Correct interpretation of estimated angles requires a clear and consistent angle convention. This work adopts a **standard uniform linear array (ULA) azimuth convention** consistent with the steering vector implementation used in the code.

4.1 Azimuth Angle Definition

The adopted convention is:

- $\theta = 0^\circ$ corresponds to **boresight**, i.e., the direction normal (perpendicular) to the radar front.
- Positive angles ($+\theta$) correspond to targets located on the **right-hand side** of the radar.
- Negative angles ($-\theta$) correspond to targets located on the **left-hand side** of the radar.

This convention defines the sign of the spatial phase progression across the RX antenna elements.

4.2 Steering Vector Phase Progression

For a uniform linear array with inter-element spacing d and wavelength λ, the phase contribution at RX element index $m \in \{0, 1, \ldots, M-1\}$ for a plane wave arriving from azimuth angle θ is given by

$$\phi_m(\theta) = 2\pi \frac{md}{\lambda} \sin(\theta). \tag{27}$$

The corresponding steering vector is

$$a(\theta) = \begin{bmatrix} 1 & e^{j\phi_1(\theta)} & \cdots & e^{j\phi_{M-1}(\theta)} \end{bmatrix}^T. \tag{28}$$

A positive value of $\sin(\theta)$ produces a **positive phase progression** across increasing RX indices, which corresponds to a target located to the right of the array under this convention.

4.3 Effect of RX Channel Ordering

The sign of the estimated angle depends critically on the **physical-to-logical ordering** of RX channels:

- If RX channels are ordered physically from left to right, the convention above applies directly.
- If the RX channel order is reversed, the effective phase progression changes sign, resulting in

$$\theta \rightarrow -\theta.$$

Mathematically, reversing the RX order applies a permutation matrix to the steering vector, which conjugate-reflects the array manifold and flips the angle sign.

4.4 Practical Validation

Angle convention can be validated experimentally by placing reflectors at known positions:

- A reflector placed to the right of the radar should yield a positive-angle peak.
- A reflector placed to the left should yield a negative-angle peak.
- A reflector placed directly in front of the radar should appear near $\theta = 0°$.

Such validation is essential when comparing results across different toolchains or hardware platforms.

5 Fundamental Limitations of the Infineon BGT60TR13C

While the Infineon BGT60TR13C is well-suited for compact sensing applications, its hardware architecture imposes several **fundamental limitations** on beamforming and high-resolution DOA estimation. These limitations are structural and cannot be overcome purely through signal processing.

5.1 Extremely Small Array Aperture

The radar provides only $M = 3$ RX antenna elements, forming a very small uniform linear array.

The achievable angular resolution is fundamentally limited by the array aperture and can be approximated as

$$\Delta\theta \approx \frac{\lambda}{Md}. \tag{29}$$

With only three elements:

- The mainlobe width is inherently large.
- Closely spaced targets cannot be reliably separated.
- Sidelobe control is poor and unstable.

As a result, all beamforming methods on this platform are **aperture-limited**, regardless of algorithmic complexity.

5.2 No Virtual Array Capability

The BGT60TR13C operates as a **single-TX, multi-RX FMCW radar**:

- One transmit antenna
- No time-division multiplexing (TDM-MIMO)
- No phase diversity across transmit channels

Because of this architecture:

- No virtual antenna elements can be synthesized.
- The effective array size is fixed at three physical RX channels.
- Classical MIMO-based aperture expansion is not possible.

Virtual channels cannot be created on this hardware platform.

This severely limits both angular resolution and the maximum number of resolvable sources.

5.3 Near-Field Effects and Model Mismatch

Many practical targets detected by the BGT60TR13C are located at short ranges where the **far-field (plane-wave) assumption** is violated.

Subspace-based methods such as MUSIC assume:

- Far-field propagation
- Plane-wave arrivals across the array
- A stationary array manifold

When targets are in the near field:

- Steering vectors become inaccurate.
- Signal and noise subspaces are no longer orthogonal.
- Spurious peaks and unstable DOA estimates appear.

These effects are particularly pronounced in indoor and laboratory environments.

5.4 Mutual Coupling and Calibration Uncertainty

Due to the compact antenna layout:

- RX elements are closely spaced.
- Mutual coupling between antennas is non-negligible.
- Element radiation patterns deviate from ideal assumptions.

Additionally, no factory-provided calibration matrix is available for:

- RX gain mismatch
- RX phase mismatch

These imperfections distort the true array manifold, reducing the effectiveness of adaptive and subspace-based beamforming methods.

5.5 Practical Implications

Because of the combined effects above, the Infineon BGT60TR13C should be viewed as:

- **Unsuitable for high-precision beamforming**
- **Marginal for subspace methods such as MUSIC**
- **Well-suited for education, prototyping, and qualitative angular awareness**

High-resolution DOA estimation generally requires:

- Larger physical arrays
- MIMO-based virtual apertures
- Accurate array calibration
- Controlled propagation environments

6 Conclusion

This work presented a complete beamforming pipeline for the Infineon BGT60TR13C FMCW radar, including range processing, spatial covariance estimation, and classical as well as adaptive beamforming techniques.

Through both theoretical analysis and experimental results, it was shown that while advanced methods such as MVDR and MUSIC can be implemented on this platform, their performance is fundamentally constrained by the radar's small array aperture, lack of virtual channels, and sensitivity to model mismatch.

Consequently, the BGT60TR13C is best utilized as a platform for:

- Educational demonstrations of array signal processing concepts
- Qualitative angular awareness
- Prototyping and algorithm development

rather than as a solution for high-resolution DOA estimation or multi-target angular separation.